Dielectric thermally conductive boron nitride/silica@MWCNTs/polyvinylidene fluoride composites via a combined electrospinning and hot press method

Zijian Wu[1,2,3], Shunying Gao[1], Xuefei Wang[1], Mohamed M. Ibrahim[4], Gaber A. M. Mersal[4], Juanna Ren[5], Zeinhom M. El-Bahy[6], Ning Guo[1,2,*], Junguo Gao[1,2,*], Ling Weng[1,2,*], and Zhanhu Guo[3,*] [ID]

[1] *School of Materials Science and Chemical Engineering, Harbin University of Science and Technology, Harbin 150040, China*

[2] *Key Laboratory of Engineering Dielectric and Its Application Technology of Ministry of Education, Harbin University of Science and Technology, Harbin 150040, China*

[3] *Mechanical and Construction Engineering, Faculty of Engineering and Environment, Northumbria University, Newcastle Upon Tyne NE1 8ST, UK*

[4] *Department of Chemistry, College of Science, Taif University, P.O. Box 11099, 21944 Taif, Saudi Arabia*

[5] *School of Materials Science and Engineering, Taiyuan University of Science and Technology, Taiyuan 030024, China*

[6] *Department of Chemistry, Faculty of Science, Al-Azhar University, Nasr City 11884, Cairo, Egypt*

ABSTRACT

With the development of microelectronics towards integration, miniaturization and high power, the accumulation of heat in this small space has become a serious problem. Therefore, polymer matrix composites with high thermal conductivity and electrical insulation need to be developed urgently. Here, an ordered oriented boron nitride/silicon dioxide (silica) coated multiwalled carbon nanotubes (BN/SiO$_2$@MWCNTs) thermally conductive network was constructed in a polyvinylidene fluoride (PVDF) matrix by electrostatic spinning technique, and subsequently the PVDF composites were prepared by hot-pressing. The synergistic effect of two-dimensional BN and one-dimensional MWCNTs in PVDF was investigated. It was found that the out-of-plane thermal conductivity of BN$_{30}$/SiO$_2$@MWCNTs composites reached 0.4693 Wm^{-1} K^{-1}, which was 209% higher than that of pure PVDF and 10% higher than that of BN/PVDF composites. The in-plane thermal conductivity of BN$_{30}$/SiO$_2$@MWCNTs) composites reached 1.5642 Wm^{-1} K^{-1}, which was 1055% higher than pure PVDF and 40% higher than BN/PVDF composites. This is attributed to the synergistic effect of BN on SiO$_2$@MWCNTs. Meanwhile, the volume resistivity and breakdown strength of the

Address correspondence to E-mail: tad@hrbust.edu.cn; gaojunguo@hrbust.edu.cn; l.weng@hrbust.edu.cn; zhanhu.guo@northumbria.ac.uk

E-mail Addresses: zijian.wu@hrbust.edu.cn

🕥 Springer

BN/SiO$_2$@MWCNTs/PVDF composites reached 3.6×10^{13} Ω m and 47.68 kV/mm, respectively. The results indicate that the BN$_{30}$/SiO$_2$@MWCNTs/PVDF composites have excellent thermal conductivity and electrical insulating properties, which are promising for microelectronics applications.

1 Introduction

In recent years, with the rapid development of electronics technology [1–3], electronic devices [4–9] have tended towards miniaturization, high integration, and high power [10–14]. Consequently, issues related to heat resistance and heat dissipation have become bottlenecks constraining the development of microelectronics technology [15–18]. Due to the highly disordered orientation of polymer molecular chains, phonon propagation processes result in significant scattering. The thermal conductivity of most polymers is far below 1 W/m k. In the field of polymer electronic packaging, enhancing the thermal conductivity of material systems is one of the core issues that urgently need to be addressed [19–21], while also considering parameters such as the electromagnetic shielding performance of materials [22–28].

Multiple approaches have been proven effective in enhancing the thermal conductivity of polymer systems, such as achieving ordered alignment of molecular chains through molecular structure design and molding condition control; introducing phase change materials [29, 30]; incorporating thermal conductive fillers [31], and so forth. Due to its simplicity, the method of introducing thermal conductive fillers is widely used in both industry and academia. Common thermal conductive fillers include: metallic materials (silver [32–34], copper [35], etc.), ceramic materials (boron nitride (BN) [36–40], aluminum oxide [37], aluminum nitride [41], SiC [42], etc.), MOF [30] and carbon materials (carbon nanotubes [43–47], graphite [48], graphene [49–51], carbon fibers [52, 53], etc.). Among these thermally conductive fillers, carbon nanotubes (about 5000 W/(m k)) and graphene (more than 1500 W/(m k)) have gained a lot of attention from scholars due to their excellent thermal conductivity [54, 55]. Kumar prepared MWCNT/epoxy composites with different mass fractions by solution mixing technique. The thermal conductivity of the composites with 1 wt% MWCNT, the thermal conductivity reached 0.9 W/m k, which was nearly 197% higher than that of the pure epoxy resin. Huynh Mai Duc [56] prepared modified MWCNT/polyurethane composites containing different mass fractions by a molding process. The thermal conductivity of the composites was 0.08 W/(m k) at 3 wt% of modified MWCNT, which was 220% higher than that of pure polyurethane (0.025 W/(m k)). Xie et al. [57] prepared modified multi-walled carbon nanotubes/epoxy composites, and found that the thermal conductivity of the composites reached 1.236 W/(m k) at 2 wt% of the modified filler. From these literatures, it can be obtained that MWCNT can effectively improve the thermal conductivity of polymer matrix composites. Despite the excellent thermal conductivity of graphene and carbon nanotubes, their electrical conductivity limits their application in insulation. Therefore, some research teams conduct surface insulation treatment on conductive fillers such as carbon nanotubes to obtain fillers that possess both high thermal conductivity and electrical insulation [44, 45].

However, it is not always possible to improve the thermal conductivity of polymers by filling them with high thermal conductivity fillers. This is because the thermal conductivity of polymers is affected by many factors, such as the micro-structure of the polymer itself, the interfacial compatibility between the polymer and the filler, and the dispersion of the filler in the matrix [58]. It has been mentioned above that polymers have low thermal conductivity due to problems such as highly disordered orientation of their molecular chains, so their thermal conductivity can be improved by increasing the crystallinity of the polymer, in general, the higher the crystallinity of the polymer, the higher its thermal conductivity. The larger interfacial thermal resistance exists in the interface between the filler and the substrate. The filler is inorganic, while the polymer is organic, and the compatibility between the filler and the polymer is not good, then the interfacial interaction between the filler and the substrate will be very poor, and the phonons will be severely scattered at this interface. Therefore, there are a large number of studies on the modification of fillers [59–61], and the modification of fillers with non-covalent modification [62] and covalent modification [63, 64]. Non-covalent modification does not damage the surface of the filler and makes

the intrinsic thermal conductivity of the filler decrease, but this method has problems such as weak force and instability [65]. Covalent modification can make up for the problems caused by non-covalent modification, but covalent modification causes defects on the surface of the filler, which leads to a decrease in the intrinsic thermal conductivity of the filler. According to the thermal network theory, the formation of a stable, large number of continuous pathways in the polymer by the filler is a key factor in improving the thermal conductivity of polymers [66]. However, the formation of a considerable amount of continuous thermally conductive pathways is highly dependent on the dispersion of the fillers. In addition, in order to form thermally conductive paths in the polymer matrix, a high content of fillers needs to be added, which in turn inevitably deteriorates the processability of polymer matrix composites. Therefore, there is an urgent need for a method that allows the thermal conductivity of polymers to be well-improved at relatively low addition levels.

BN, as a kind of ceramic filler, has gained wide attention in the field of insulation because of its good insulating properties, although its thermal conductivity is not particularly high (200–400 W/(m K)) compared with that of CNTs and graphene. Numerous investigations have been conducted on thermally conductive composites based on BN polymers, along with extensive research focusing on the surface modification of BN [67]. Numerous studies have found that introducing thermal fillers of different sizes and dimensions (0D, 1D and 3D) into resin matrices exhibits significant synergistic effects in enhancing the thermal conductivity and other properties of composite materials. Liu et al. prepared BN/alumina/ polydimethylsiloxane composites by 3D printing technique, the thermal conductivity of oriented BN/ Al_2O_3/PDMA composites was higher than that of the random BN/Al_2O_3/PDMS composites. The in-plane thermal conductivity of the composites oriented with 35 wt% BN and 30 wt% alumina mixed filler reached 3.64 W/(m k), where BN acted as a fast heat transfer in the matrix and spherical alumina acted as a reinforcement of the filler network. Fan [68] prepared alumina/ BN/epoxy composites, after the addition of alumina to BN/epoxy composites, the thermal conductivity of alumina/BN/epoxy was higher than that of composite materials with randomly dispersed thermal particles. After adding alumina to BN/epoxy resin, the thermal conductivity of alumina/BN/epoxy resin composites

was higher than that of BN/epoxy resin composites. Isarn [69] prepared carbon nanotube/BN/epoxy resin composites. The above literature shows that co-doping of one-dimensional fillers with two-dimensional fillers into polymers does result in synergistic effects and improves the processing properties of polymer matrix composites for the betterment of polymer matrix composites.

Constructing an efficient three-dimensional thermal conduction network is key to enhancing thermal conductivity while maintaining mechanical performance. Numerous techniques [70, 71] have been developed for fabricating three-dimensional network structures, including ice-templating, segregation, electrospinning, 3D printing and chemical vapor deposition. Among them, the ice-templating technique, which relies on the self-assembly induced by ice crystal growth followed by the vacuum filtration of a polymer matrix, is a commonly employed approach for constructing three-dimensional networks. Pan [72] fabricated BN whiskers (BNWK)@Al_2O_3/cellulose aerogels (CA) through electrostatic self-assembly of one-dimensional BNWK and zero-dimensional nano-Al_2O_3, combined with directional freezing of CA. The resulting BNWK@ Al_2O_3/CA composite not only possesses a distinctive vertical network structure but also demonstrates remarkable compressive mechanical strength. The thermal conductivity of the epoxy-based composite (BNWK@Al_2O_3/CA/EP) with a filler loading of 8.6 wt% is approximately 1.92 W/(m·K).

In this work, poly(vinylidene fluoride) (PVDF) was chosen as the matrix owing to its exceptional thermal stability and durability. Moreover, it lends itself to seamless processing through injection molding or melting techniques. Notably non-toxic and endowed with resistance to both heat and chemicals, PVDF exhibits minimal water absorption, rendering it an ideal candidate for the production of electronic components [73]. Boron nitride and multi-walled carbon nanotubes were incorporated into poly(vinylidene fluoride) (PVDF), with subsequent coating of the multi-walled carbon nanotubes with silica, aiming to preserve the insulating characteristics inherent to PVDF. The electrostatic spinning technique was employed to construct an ordered BN/SiO_2@MWCNT thermally conductive network in PVDF, and then combined with the hot-pressing technique, the compact composites were prepared. Electrospinning technology can arrange thermal conductive fillers along the direction of fibers, thus constructing efficient thermal

conduction networks. Compared to the ice-templating method, electrospinning technology eliminates the need for directional freezing and freeze-drying equipment, making it easier to achieve scalable production of large-sized samples. It was found that this method significantly enhanced the thermal conductivity of the PVDF composites, while also positively influencing their electrical and mechanical properties.

2 Experiment

2.1 Materials

The polyvinylidene fluoride (761A, diameters in the range of 10–20 nm) used in this work was from Shijiazhuang Xinlongwei Chemical Co. Ltd; multi-wall carbon nanotubes (length > 5 μm, purity > 97%) was purchased form Shenzhen NanoPort Co. Born nitride (purity > 98.5%) was purchased from Shanghai McLean Biochemical Technology Co., Ltd; silica-coated multi-walled carbon nanotubes were homemade; *N′N*-dimethylformamide (DMF) was purchased from Tianjin Fuyu Fine Chemical Co.

2.2 Sample preparations

2.2.1 Preparation of spinning solution

As shown in Fig. 1, a certain amount of BN and SiO$_2$@MWCNT was added to a three-necked flask (the addition of SiO$_2$@MWCNTs was fixed at 1 wt%), followed by the addition of DMF and acetone (w:w = 7:3), and

then, after sonication for 1 h, the PVDF powders were then added to the three-necked flasks, and the spinning solution was obtained by stirring for 2 h at 40 °C.

2.2.2 Preparation of composite materials

As shown in Fig. 2, the prepared spinning solution was injected into the syringe. The suitable sized aluminum foil was laid flat on the receiver and a uniform layer of insulating silicone grease was applied on the surface. The voltage was set to 15 kV, the advance rate of the syringe was set to 13 μl/min, and the needle was 15 cm away from the drum receiver. The spun film was then placed in an oven at 80 °C for 3 h to remove the solvent. After solvent removal, the spun films were hot pressed at 180 °C for 20 min at 10 MPa using a plate vulcanizer to obtain BN/SiO$_2$@MWCNTs/PVDF composites. The prepared samples were named "BN$_x$/SiO$_2$@MWCNTs/PVDF", and the subscript *x* refers to the mass fraction of boron nitride in PVDF, and the mass fraction of silica-coated multi-walled carbon nanotubes was fixed at 1 wt%.

2.3 Performance testing

2.3.1 Micro-characterization

A transmission electron microscope (TEM) HT-7700 was used to characterize the fibers of BN/SiO$_2$@MWCNT/PVDF composites. (Samples were collected during electrostatic spinning using a copper mesh under a needle to receive the fibers.) A scanning
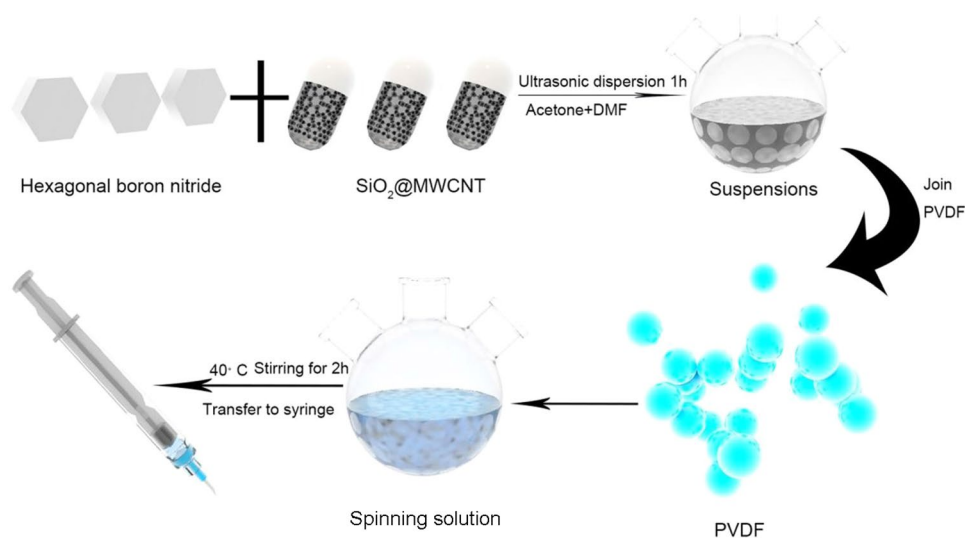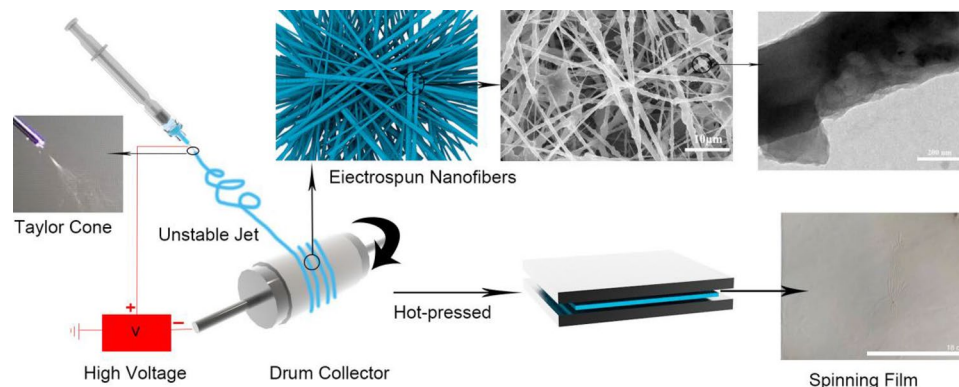
Fig. 1 Preparation process of spinning solution

Fig. 2 Preparation of BNx/SiO$_2$@MWCNTs/PVDF composites

electron microscope (SEM) FEI Sirion 200 was used to observe the surface morphology of the spun film. The structure of BN/SiO$_2$@MWCNTs/PVDF composites was characterized using X-ray diffractometer (XRD). The test range was $2\theta = 10°–80°$.

2.3.2 Dielectric properties testing

The dielectric constant, dielectric loss, and conductivity of the composites were tested using a broadband dielectric impedance spectrometer (Alpha-A) in the frequency range of 10^2 to 10^7 Hz at room temperature.

2.3.3 Bulk resistivity test

The volume resistivity of the composites was tested at room temperature using a high resistance meter (ZC36).

2.3.4 Breakdown field strength test

The breakdown field strength of the composites was tested using a breakdown tester (HT-100), 8 times per sample. The samples were analyzed using a two-parameter Weibull distribution function.

2.3.5 Dynamic thermo-mechanical property testing

The dynamic thermo-mechanical properties of the composites were tested using a DMA Dynamic Thermo-mechanical Analyzer (Q800) in the temperature range of 30–170 °C.

2.3.6 Thermal conductivity test

The surface of the samples was carbon sprayed according to ASTM-E1461 and the thermal conductivity of the composites was tested at room temperature using a laser thermal conductivity meter LFA-447. According to the equation of $\lambda = a*\rho*C_p$, where a (mm^2/s), ρ (g/cm^3), and C_p (J/g/K) correspond to the thermal difusivity, density, and specifc heat capacity of the sample, respectively.

3 Results and analysis

3.1 Micro-characterization analysis

Figure 3b–d shows SEM images of BN/SiO$_2$@MWC-NTs/PVDF spun films with different BN contents. It can be seen from these plots that the fillers are oriented along the fibre direction. This is a visual evidence that PVDF contains a thermally conductive network orientated along the plane. The reason that the addition of thermally conductive fillers to PVDF results in an increase in the thermal conductivity of the composite is because the fillers form thermally conductive pathways in the matrix, allowing phonons to be rapidly conducted through these pathways. As the filler content increases, the better the thermal network built in the composite, and therefore the thermal conductivity of the composite will be higher. It can be visualized in Fig. 3b–d that the thermal conductivity network in the BN$_{30}$/SiO$_2$@MWCNTs composites is the most complete. The BN and SiO$_2$@MWCNTs are connected (Fig. 4b), which proves that the BN$_{30}$/SiO$_2$@MWCNTs composites contain a continuous thermal conductivity

Fig. 3 SEM image of spun film of PVDF and PVDF composites. **a** PVDF, **b** BN$_{10}$/SiO$_2$@MWCNTs/PVDF, **c** BN$_{20}$/SiO$_2$@MWCNTs/PVDF, **d** BN$_{30}$/SiO$_2$@MWCNTs/PVDF
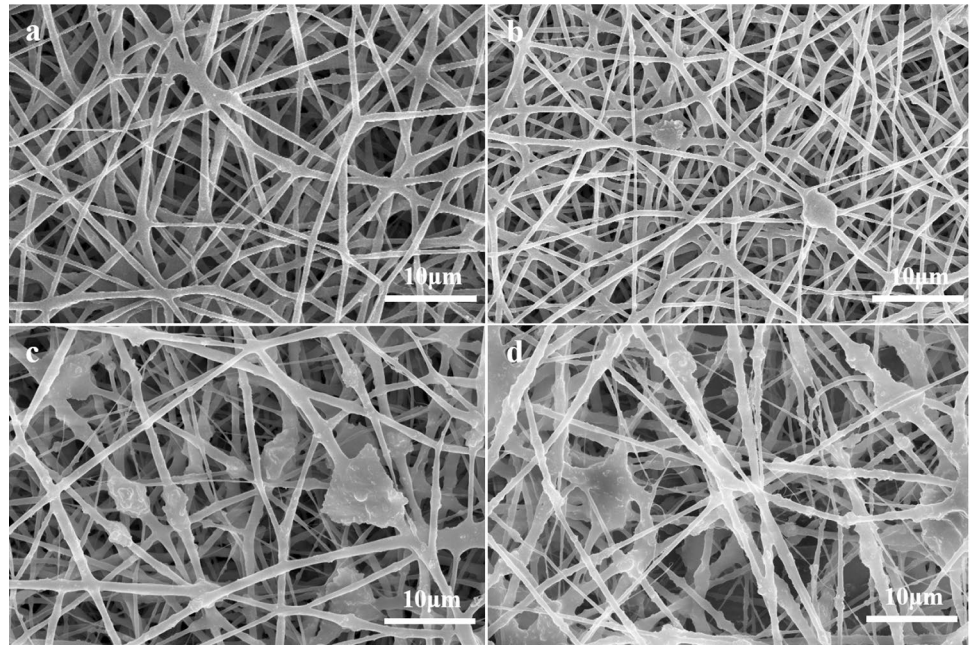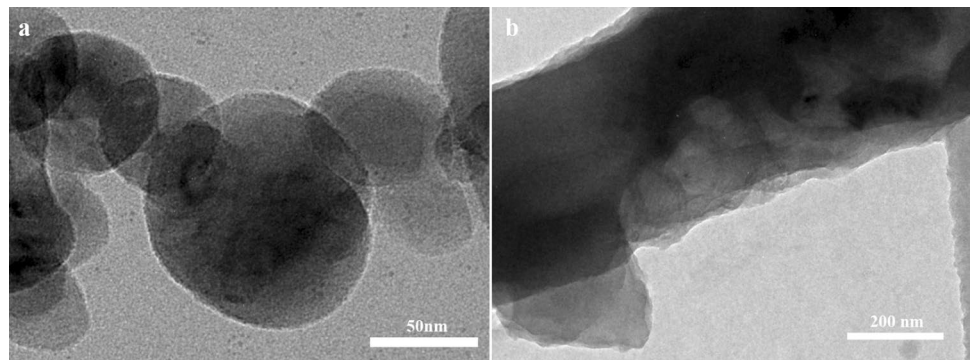

Fig. 4 **a** TEM image of BN, **b** TEM image of BN$_{30}$/SiO$_2$@MWCNTs/PVDF

network, and it is one of the most effective evidences that the thermal conductivity of the BN$_{30}$@MWCNTs composites is the highest.

The thermal conductivity of boron nitride along the plane direction is much higher than that of the through-plane, so the orientation of boron nitride in PVDF is worth investigating. XRD test can test the crystal structure of the material, and the orientation of boron nitride in PVDF can be determined with the help of this test. As shown in Fig. 5, the diffraction peaks at $2\theta = 26.7°$ and $41.6°$ correspond to the (002) and (100) crystal planes of boron nitride, respectively [74], and the intensities of the (020) and (100) crystal planes increase with the increase of boron nitride content. The high ratio of I002/I100 indicates that the boron nitride is highly planarly oriented in PVDF. The probable reason why this highly planar orientation
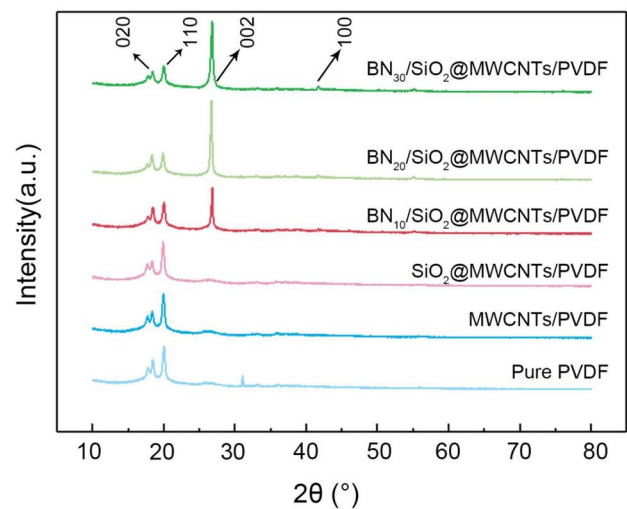

Fig. 5 XDR patterns of PVDF composites

occurs is that the large transverse size of boron nitride facilitates the orientation of boron nitride along the horizontal direction during the spinning process [75]. This orientation structure will promote the increase of thermal conductivity within the composite faces. In addition, the diffraction peaks at $2\theta = 18.4°$ and $19.9°$ are the α-phase and β-phase of the PVDF matrix, respectively [76]. Compared with PVDF, the strength ratios of the composite's (110) and (020) crystal planes decrease after the addition of boron nitride, which suggests that the addition of boron nitride to PVDF will somewhat disrupt the integrity of the crystallinity of PVDF. In addition, we can also find that the strength of (020) and (110) crystal faces is weakened compared to PVDF after adding MWCNTs, while the relative strengths of (020) and (110) crystal faces are increased compared to PVDF after adding SiO_2@MWCNTs. Due to the effect of fillers, the PVDF crystals preferentially grow towards the (110) crystal plane to form the β phase.

3.2 Analysis of dielectric properties

The dielectric constant is used to describe the macroscopic elaboration of dielectric polarisation. According to the microscopic mechanism of dielectric

polarisation, the polarisation of a dielectric can be reduced to five basic forms: electron displacement polarisation, ion displacement polarisation, steering polarisation, thermionic polarisation and interfacial polarisation. Therefore, when analysing the relative dielectric constant of the dielectric, the type of polarisation present in the dielectric should be considered comprehensively. For pure PVDF composites, the main steering polarisation occurs in PVDF under the action of the electric field, and interfacial polarisation occurs in PVDF composites in addition to steering polarisation. The composites containing MWCNTs are additionally subjected to electron displacement polarisation under the action of electric field because MWCNTs are conducting materials. Therefore at the same frequency (10^2 Hz), the dielectric constant of MWCNTs/PVDF composites is the highest and SiO_2@MWCNTs/PVDF composites are the second highest [31]. In addition the dielectric constants of BN_x/SiO_2@MWCNTs/PVDF composites are all higher than that of the pure PVDF. As seen in Fig. 6a, the dielectric constants of the composites all show a decreasing trend with increasing frequency. The reason may be that in the low-frequency region, all kinds of polarisation have time to be established, while in the high-frequency region, the steering

Fig. 6 **a** Dielectric constant and **b** dielectric loss of PVDF composites, **c** conductivity and **d** volume resistivity of PVDF composites
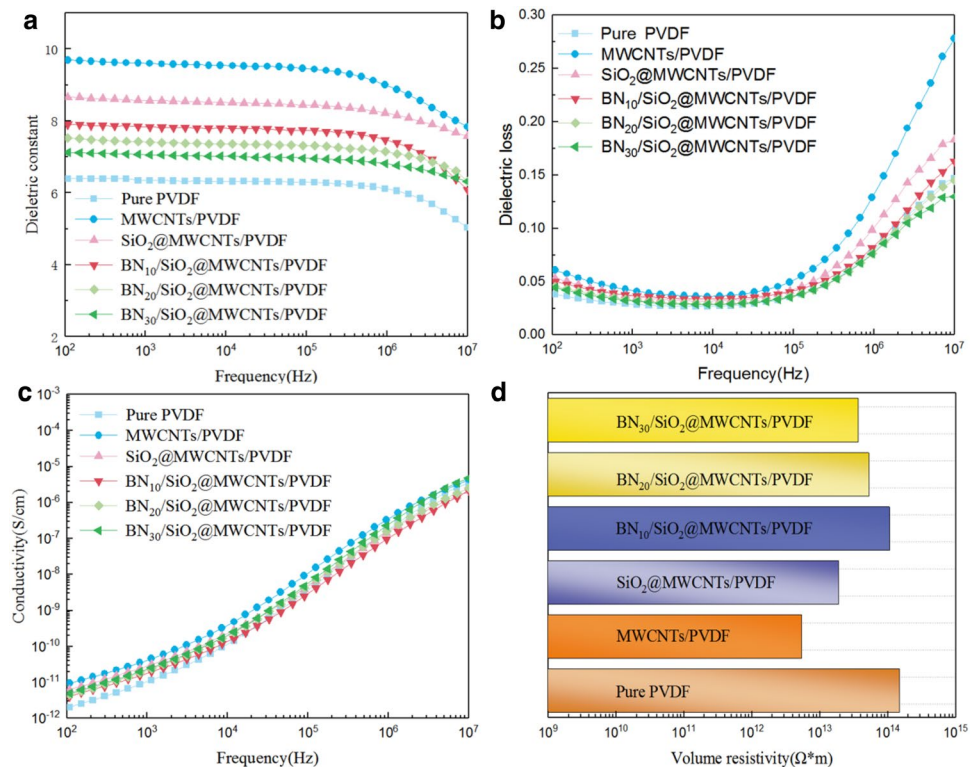
polarisation and interfacial polarisation are too late to be established, and the polarisation of the composites is all contributed by the electron displacement polarisation.

The energy consumed by the dielectric per unit time is called dielectric loss, which can be caused by conductivity and relaxation polarisation.The variation of dielectric loss with frequency for PVDF composites, SiO_2@MWCNTs/PVDF composites and BN_x/SiO_2@MWCNTs/PVDF composites is shown in Fig. 6b. The dielectric losses of both PVDF and composites show a tendency of decreasing and then increasing with increasing frequency. As mentioned above, at lower frequencies, for PVDF and PVDF composites, the steering polarisation has time to build up, so the dielectric loss is lower at this time, with the increase of frequency, the electric field change accelerates, the dipole can still undergo steering polarisation, but the time for the orientation motion decreases, and the orientational movement of the dipole becomes more intense, which leads to an increase in the dielectric loss of PVDF and PVDF composites. At high frequencies, the relaxation polarisation is too late to be established, when no relaxation loss occurs, but the increase in the number of peripheral waves per second makes the dielectric loss still increase.The direct contact between the MWCNT and the MWCNT induces higher leakage currents, and the electron displacement polarisation is more likely to occur under the action of the electric field. Therefore, from Fig. 6b, it can be observed that the dielectric loss of MWCNTs/PVDF composites is higher than that of PVDF, and also the surface of MWCNT is coated with SiO_2, which can inhibit the electron migration to a certain extent due to the insulating property of SiO_2, so the dielectric loss of SiO_2@MWCNTs/PVDF composites is less than that of MWCNTs/PVDF composites. After the addition of BN in SiO_2@MWCNTs/PVDF composites, BN further prevented the contact of MWCNTs and reduced the dielectric loss of the composites. In Fig. 6c, the electrical conductivity of MWCNTs/PVDF composites is higher than that of other composites and pure PVDF, which is related to the nature of the filler itself, and the addition of insulating BN to SiO_2@MWCNTs/PVDF composites further prevents the contact between MWCNTs, so the electrical conductivity of composites containing SiO_2@MWCNTs and BN/SiO_2@MWCNTs will be lower than that of MWCNTs. and BN/SiO_2@MWCNTs will have lower electrical conductivity than MWCNTs/PVDF composites.

3.3 Volume resistivity analysis

In the field of microelectronics, it is necessary to examine the electrical properties of materials. Volume resistivity is the impedance of a material to current per unit volume and can be used to characterise the electrical properties of a material. A higher volume resistivity of a material means a better insulating property of the material. It has been demonstrated that the addition of multi-walled carbon nanotubes to PVDF results in a decrease in the volume resistivity of the composite material because the introduction of multi-walled carbon nanotubes increases the carrier concentration of the composite material [77]. This is consistent with our findings. In order to improve the volume resistivity of MWCNTs/PVDF composites, in this paper, a layer of SiO_2 was coated on the surface of MWCNTs, and as expected, the volume resistivity of SiO_2@MWCNTs/PVDF composites was higher than that of MWCNTs/PVDF composites. This is due to the fact that SiO_2 is insulating, which inhibits carrier migration and reduces the leakage current. Also adding different contents of boron nitride to the SiO_2@MWCNTs/PVDF composites, it was found that the volume resistivity of the composites tended to decrease with the increase of the boron nitride content (as shown in Fig. 7), which may be due to the poor interfacial compatibility between BN and PVDF, and the formation of voids and defects between BN and PVDF. The aggregation of boron nitride in the PVDF matrix is demonstrated
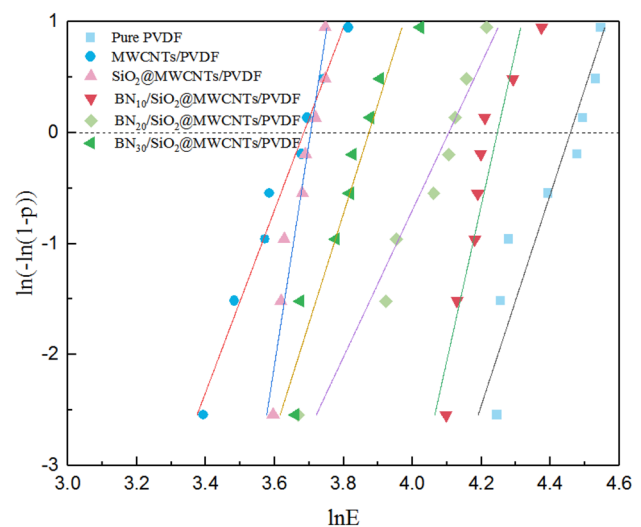

Fig. 7 Weibull distribution of PVDF composites

to us in Fig. 3. As the BN content increases, the more defects are found in the matrix.

3.4 Breakdown field strength analysis

Breakdown field strength is also an important parameter for evaluating the insulating properties of a material, which reflects the resistance of the solid dielectric itself. Therefore, it is necessary to test the breakdown field strength of the material. In general, the breakdown field strengths of composites are lower than that of pure PVDF, which is due to the fact that the addition of filler to PVDF introduces an interface between the filler and the matrix, and the space charge will be easily captured by the interface between the filler and the matrix [78]. In contrast, the breakdown field strengths of SiO_2@MWCNTs/PVDF composites are higher than that of MWCNTs/PVDF composites, which indicates that the SiO_2 insulating layer effectively prevents the formation of conductive pathways in MWCNTs [79]. The effect of BN on the breakdown field strength of SiO_2@MWCNTs/PVDF composites is the same as that on the volume resistivity of the composites (shown in Fig. 8). The breakdown field strength of the BN/SiO_2@MWCNTs/PVDF composites is higher than that of the SiO_2@MWCNTs/PVDF composites, partly because of the superior insulating properties of BN with a wider bandgap [80], and partly because of the incorporation of BN which prevents the formation of the conductive pathway of the SiO_2@MWCNTs to a certain extent. The calculated Weibull distribution parameters are shown in Table 1. From the table, it can be seen that the β values of the composites are relatively large, and the large β values indicate that the data obey the Weibull distribution, which also indicates that the data are less dispersed and more reliable.

Table 1 Weibull distribution parameters for breakdown field strength of PVDF composites

Sample	Shape parameter β	Breakthrough field strength E_b (kV/mm)
PVDF	10.32	86.53
MWCNTs/PVDF	8.92	39.78
SiO_2@MWCNTs/PVDF	21.32	40.63
BN_{10}/SiO_2@MWCNTs/PVDF	11.20	70.28
BN_{20}/SiO_2@MWCNTs/PVDF	8.65	60.22
BN_{30}/SiO_2@MWCNTs/PVDF	9.18	48.27

3.5 Analysis of dynamic thermo-mechanical properties

Energy storage modulus is the ability of a material to store energy, reflecting the stiffness and elasticity of the material. When the material is subjected to an external force, the stored energy can restore the material to its original shape. Loss modulus is the ability of a material to consume energy during vibration or deformation, reflecting the viscosity and elasticity of the material. When a material is subjected to an external force, the lost energy can cause it to heat up or deform. The mechanical properties of a material can change significantly with the addition of inorganic particles. The energy storage modulus and loss modulus of (BN_{30}/SiO_2@MWCNTs/PVDF) composites were found to be 3452.4 Mpa/137.2 Mpa, respectively, at 30 °C. As expected, the energy storage modulus of the composites was higher than that of the pure polymer as shown in Fig. 8a. This indicates that the rigid filler changes the viscoelastic properties of the polymer. When the temperature is low, the rigid filler restricts the movement of the polymer chains and

Fig. 8 **a** Storage modulus and **b** loss modulus of composites
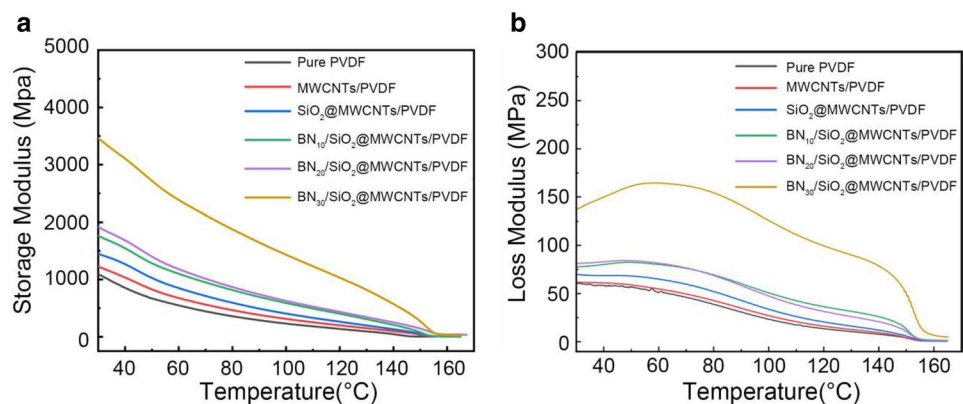
becomes stronger with the increase of filler content. Also the energy storage modulus and loss modulus of SiO$_2$@MWCNTs/PVDF composites are higher than those of MWCNTs/PVDF composites. This is due to the good interfacial compatibility between SiO$_2$@MWVNTs and PVDF composites at the same content, which plays a greater role in restricting the movement of polymer molecular chains. When the temperature increases, the polymer chain mobility is enhanced and the filler loses its role in restricting the movement of the polymer. The trend of loss modulus though fillers is similar to the energy storage modulus, as the filler content increases, the more energy the polymer has to overcome.

3.6 Thermal conductivity analysis

Polymers have low intrinsic thermal conductivity due to the high degree of disorder in their molecular chains and the high scattering of phonons in the polymers. Adding high thermal conductivity fillers to polymers is one of the effective strategies to improve the thermal conductivity of polymers. According to the thermal pathway theory, the better the thermal network formed by the filler in the matrix, the higher the thermal conductivity of the polymer matrix composites. In addition, the thermal conductivity of polymer matrix composites is affected by the crystalline state of the polymer, filler content, orientation, dispersion state, and interfacial interactions between the filler and the matrix [81]. By means of electrostatic spinning, the thermally conductive fillers can be made to be oriented in the matrix, resulting in an anisotropic thermal conductivity for the polymer matrix (the out-of-plane thermal conductivity for the BN$_{30}$/MWCNTs/PVDF composite is 0.5081 Wm^{-1} K^{-1} (235% higher than

that of PVDF), and the in-plane thermal conductivity is 1.7523 Wm^{-1} K^{-1} (1055% higher than that of PVDF)), which is due to the fact that the fillers will be oriented along the direction of the fibres during spinning, and the fibres are stacked one on top of another, so that the fillers will be oriented along the planar surface, and the one-dimensional fillers will be bridged to the two-dimensional fillers, so that the filler will be able to form a more effective thermal conductivity network, and the phonons will be transferred along the path of least thermal resistance, so that the filler will be able to transfer the heat from the surface of the polymer matrix. Will travel along the path of least thermal resistance, so that heat can travel faster in the planar direction, resulting in higher in-plane thermal conductivity, which is higher than out-of-plane thermal conductivity. As expected, the in-plane and out-of-plane thermal conductivities of BN$_x$/PVDF composites, BN$_x$/MWCNTs/PVDF composites and BN$_x$/SiO$_2$@MWCNTs/PVDF composites increased with the increase of BN content (as shown in Fig. 9). This is due to the fact that with the increase of filler content, there are more opportunities for filler to filler contact, which leads to a better thermal conductivity pathways.

4 Conclusion

The in-plane and out-of-plane thermal conductivity of the BN/SiO$_2$@MWCNTs/PVDF with 30 wt% BN were 1.5642 Wm^{-1} K^{-1} and 0.4693 Wm^{-1} K^{-1}, respectively. The volume resistivity and breakdown field strength of BN$_{30}$/SiO$_2$@MWCNTs/PVDF composites were 3.6 × 10^{13} Ω m and 47.68 kV/mm, respectively. The volume resistivity as well as the breakdown field strength were decreased compared with that of PVDF, but still

Fig. 9 a In-plane and **b** Out-of-plane thermal conductivity of composites
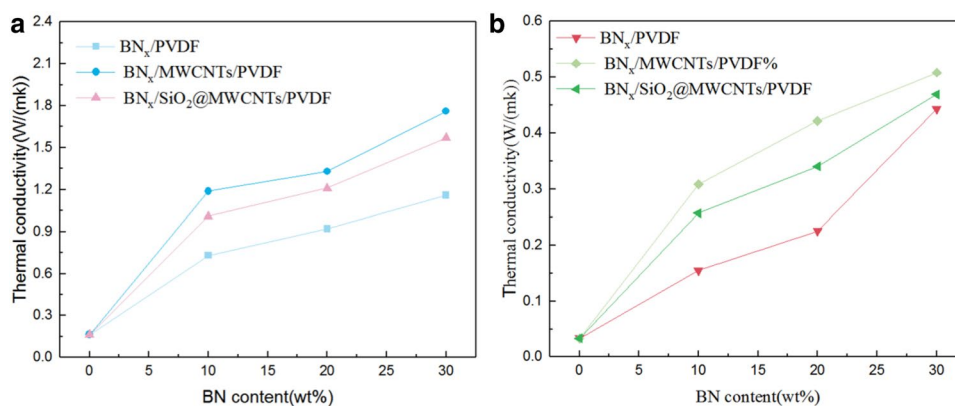
maintains electrical insulation. The synergistic effect of the one-dimensional SiO_2@MWCNTs core–shell structure and the two-dimensional BN ensures the insulation of the composite material. The energy storage modulus and loss modulus of the BN_{30}/SiO_2@MWCNTs/PVDF composites were improved obviously. Achieving simultaneous improvement in thermal conductivity and mechanical performance while maintaining the insulation properties of composite materials demonstrates the excellent synergistic effect between one-dimensional carbon nanotube core–shell structure and two-dimensional BN. The design strategy of such composites may be applicable in areas such as electronic packaging, thermal-interface materials, wearable devices, battery thermal management.

Author contributions

Zijian Wu and Shunying Gao: Methodology, Supervision, Investigation, Formal analysis, Writing—original draft. Mohamed M. Ibrahim and Gaber A. M. Mersal: Writing—review and editing. Juanna Ren: Formal analysis. Zeinhom M. El-Bahy and Junguo Gao: Writing—review and editing. Ning Guo and Ling Weng: Supervision, Resources, Writing—review and editing. Zhanhu Guo: Investigation, Resources, Writing—review and editing.

Data availability

Data will be available upon request.

Declarations

References

1. S. Tang, A. Juan, D. Drysdale, J.D. Menjivar, J. Guzman, ES Mater. Manuf. **17**, 57 (2022)
2. R. Zhang, C. Chen, H. Yu et al., J. Electroanal. Chem. **893**, 115323 (2021)
3. D. Hao, T. Chen, P. Guo et al., Adv. Compos. Hybrid Mater. **6**, 129 (2023)
4. Y. Hu, Y.H. Gong, H.H. Zeng, J.H. Wang, X.L. Fan, Phys. Chem. Chem. Phys. **22**, 24506 (2020)
5. C. Hu, F. Wang, X. Cui, Y. Zhu, Adv. Compos. Hybrid Mater. **6**, 70 (2023)
6. J. Wang, L. Su, X. Wei, R. Zheng, Y. Hu, J. Instrum. **10**, T09006 (2015)
7. H. Wang, X. Guo, X. Zhao, G. Dong, Adv. Compos. Hybrid Mater. **6**, 17 (2022)

8. V.K. Pandit, N.M. Soudagar, M.V. Mandke, S.S. Joshi, ES Gener. **3**, 1058 (2024)

9. S. Vyas, A. Shukla, S. Shivhare, R. Das, R. Venkatesh, ES Mater. Manuf. **23**, 1002 (2024)

10. F. Ye, Z. Yan, H. Zhang, H. Chang, P. Neuzil, Trends Anal. Chem. **126**, 115858 (2020)

11. J. Tang, S. Wu, N. AlMasoud et al., Adv. Compos. Hybrid Mater. **6**, 155 (2023)

12. Y. Wang, H. Zhu, J. Feng, P. Neuzil, Trends Anal. Chem. **143**, 116353 (2021)

13. X. Zhao, Y. Du, W. Li, Z. Zhao, M. Lei, Adv. Compos. Hybrid Mater. **6**, 176 (2023)

14. C. Mahata, J. Pyo, B. Jeon, M. Ismail, J. Moon, S. Kim, Adv. Compos. Hybrid Mater. **6**, 144 (2023)

15. D.P. Jiang, J.K. Yu, RSC Adv. **9**, 34677 (2019)

16. S. Jambhulkar, D. Ravichandran, V. Thippanna, D. Patil, K. Song, Adv. Compos. Hybrid Mater. **6**, 93 (2023)

17. R. Liu, J.G. Kim, P. Dhakal et al., Adv. Compos. Hybrid Mater. **6**, 14 (2022)

18. N. Guler, M. Salamah, Eng. Sci. **25**, 932 (2023)

19. Z.F. Wang, Z.J. Wu, L. Weng et al., Adv. Funct. Mater. **33**, 2301549 (2023)

20. C.G. Zhao, Y.F. Li, Y.C. Liu, H.Q. Xie, W. Yu, Adv. Compos. Hybrid Mater. **6**, 27 (2023)

21. J. Sun, X. Zhang, Q. Du, V. Murugadoss, D. Wu, Z. Guo, ES Mater. Manuf. **13**, 53 (2021)

22. H.R. Cheng, L.L. Xing, Y. Zuo et al., Adv. Compos. Hybrid Mater. **5**, 755 (2022)

23. Z. Leng, Z.Y. Yang, X.X. Tang et al., Adv. Compos. Hybrid Mater. **6**, 195 (2023)

24. D. Skoda, J. Vilcakova, R.S. Yadav et al., Adv. Compos. Hybrid Mater. **6**, 113 (2023)

25. L. Wang, J.W. Cheng, Y.X. Zou et al., Adv. Compos. Hybrid Mater. **6**, 172 (2023)

26. P. Wang, L. Yang, J.C. Ling et al., Adv. Compos. Hybrid Mater. **5**, 2066 (2022)

27. Y.F. Wu, K. Huang, X.D. Weng et al., Adv. Compos. Hybrid Mater. **5**, 71 (2022)

28. S.A. Zheng, N. Wu, Y. Liu et al., Adv. Compos. Hybrid Mater. **6**, 161 (2023)

29. H. Wang, J. Dang, M.Z. Zheng, Y.H. Yuan, T. Liu, N. Wang, Adv. Compos. Hybrid Mater. **6**, 165 (2023)

30. H. Xu, M. Zu, H. Cheng, D. Liu, W. Xie, Adv. Compos. Hybrid Mater. **5**, 2896 (2022)

31. M. Li, M. Wang, X. Hou et al., Compos. B **187**, 107746 (2020)

32. D. Jiang, Y. Wang, B. Li et al., Macromol. Mater. Eng. **304**, 1900074 (2019)

33. M. Seol, U. Hwang, J. Kim et al., Adv. Compos. Hybrid Mater. **6**, 46 (2023)

34. C.M. Wu, L.J. Zeng, G.J. Chang et al., Adv. Compos. Hybrid Mater. **6**, 31 (2023)

35. H. Yuan, Y. Wang, T. Li et al., Compos. Sci. Technol. **164**, 153 (2018)

36. Y. Sun, H. Dang, H. Tan, J. Luan, D. Jiang, Y. Yang, Macromol. Mater. Eng. **306**, 2100532 (2021)

37. D.C. Hu, H.Q. Liu, M.Z. Yang, Y.K. Guo, W.S. Ma, Adv. Compos. Hybrid Mater. **5**, 3201 (2022)

38. D. Zhang, M. Zhang, J. Wang et al., Adv. Compos. Hybrid Mater. **5**, 1812 (2022)

39. J.W. Ren, G.Q. Jiang, Z. Wang et al., Adv. Compos. Hybrid Mater. **7**, 5 (2024)

40. G. Zhao, F. Qian, X. Li et al., Adv. Compos. Hybrid Mater. **6**, 184 (2023)

41. H. Joo, Y. Lee, J. Kim et al., Sci. Adv. **7**, eabg4639 (2021)

42. M. Clausi, M. Zahid, A. Shayganpour, I.S. Bayer, Adv. Compos. Hybrid Mater. **5**, 798 (2022)

43. Z. Wang, Z. Wu, N. AlMasoud et al., Adv. Compos. Hybrid Mater. **6**, 125 (2023)

44. Z. Wu, S. Gao, L. Chen et al., Macromol. Chem. Phys. **218**, 1700357 (2017)

45. Z. Wu, X. Wang, S.H.K. Annamareddy et al., ES Mater. Manuf. **22**, 847 (2023)

46. X. Yu, Z. Wu, L. Weng et al., Adv. Mater. Interfaces **10**, 2202292 (2023)

47. M.Y. Zhang, Z.H. Zhai, M.C. Li et al., J. Compos. Mater. **50**, 3363 (2016)

48. T. Hirahara, RSC Adv. **8**, 16781 (2018)

49. X.Y. Liu, X.H. Lv, Q.F. Tian et al., Adv. Compos. Hybrid Mater. **6**, 141 (2023)

50. A. Osman, A. Elhakeem, S. Kaytbay, A. Ahmed, Adv. Compos. Hybrid Mater. **5**, 547 (2022)

51. N. Song, F. Zhang, D.L. Cao, P. Wang, P. Ding, Adv. Compos. Hybrid Mater. **5**, 2873 (2022)

52. Z.J. Wu, H.Y. Cui, L. Chen et al., Compos. Sci. Technol. **164**, 195 (2018)

53. H. Zhang, X.W. Zhang, D.T. Li et al., Adv. Compos. Hybrid Mater. **5**, 1756 (2022)

54. R.H. Sun, H. Yao, H.B. Zhang, Y. Li, Y.W. Mai, Z.Z. Yu, Compos. Sci. Technol. **137**, 16 (2016)

55. A. Oluwalowo, N. Nguyen, S.L. Zhang, J.G. Park, R. Liang, Carbon **146**, 224 (2019)

56. H.M. Duc, D.N. Huu, T.T. Huu et al., Adv. Polym. Technol. **2021**, 1 (2021)

57. F. Xie, S. Qi, R. Yang, D. Wu, J. Appl. Polym. Sci. **132** (2014)

58. X. Xu, J. Chen, J. Zhou, B. Li, Adv. Mater. **30**, e1705544 (2018)

59. F. Xie, S.H. Qi, R. Yang, D. Wu, J. Appl. Polym. Sci. **132**, 41255 (2015)

60. X. He, S. Li, R. Shen et al., Adv. Compos. Hybrid Mater. **5**, 1699 (2022)

61. J. Yang, L. Tong, A.S. Alsubaie et al., Adv. Compos. Hybrid Mater. **5**, 834 (2022)

62. Q. Yan, X. Cui, H. He, M. El-Khouly, B. Zhang, Y. Chen, Adv. Compos. Hybrid Mater. **6**, 52 (2023)

63. Z. Li, C. Wang, T. Liu et al., Adv. Compos. Hybrid Mater. **6**, 69 (2023)

64. K. Hou, X. Xu, Y. Xiang et al., Adv. Compos. Hybrid Mater. **6**, 77 (2023)

65. M.R. Nobile, M. Raimondo, C. Naddeo, L. Guadagno, Nanomaterials **10**, 1310 (2020)

66. Z.-G. Wang, F. Gong, W.-C. Yu et al., Compos. Sci. Technol. **162**, 7 (2018)

67. W.R. Zhang, Y.D. Wang, H.L. Sun, C.T. Liu, C.Y. Shen, X.H. Liu, Adv. Compos. Hybrid Mater. **6**, 163 (2023)

68. F. Su, L. Zhang, C. Li, Polym. Compos. **42**, 3562 (2021)

69. I. Isarn, L. Bonnaud, L. Massagués, À. Serra, F. Ferrando, Prog. Org. Coat. **133**, 299 (2019)

70. C. Zhao, Y. Li, Y. Liu, H. Xie, W. Yu, Adv. Compos. Hybrid Mater. **6**, 27 (2022)

71. P. Lian, R. Yan, Z. Wu et al., Adv. Compos. Hybrid Mater. **6**, 74 (2023)

72. Z. Li, D. Pan, Z. Han et al., Adv. Compos. Hybrid Mater. **6**, 224 (2023)

73. W. Zhou, J. Zuo, W. Ren, Compos. A **43**, 658 (2012)

74. M. Ghanbarian, E. Taheri Nassaj, A. Kariminejad, Surf. Coat. Technol. **288**, 185 (2016)

75. D.-L. Zhang, J.-W. Zha, W.-K. Li et al., Compos. Sci. Technol. **156**, 1 (2018)

76. Y. Xie, J. Wang, Y. Yu, W. Jiang, Z. Zhang, Appl. Surf. Sci. **440**, 1150 (2018)

77. B. Hu, H. Guo, Q. Wang et al., Compos. A **137**, 106038 (2020)

78. Q. Wang, G. Chen, ITDEI **21**, 1809 (2014)

79. Y. Liu, J. Shi, P. Kang et al., Polymer **188**, 122157 (2020)

80. T. Li, Z. Tang, Z. Huang, J. Yu, Physica E **85**, 137 (2017)

81. Y. Guo, K. Ruan, X. Shi, X. Yang, J. Gu, Compos. Sci. Technol. **193**, 108134 (2020)